Controlled Design of Phase- and Size-tunable Monodisperse Ni_2P Nanoparticles in a Phosphonium-based Ionic Liquid through Response Surface Methodology (RSM)

Lucía Mora-Tamez,[1] Gözde Barim,[1] Courtney Downes,[2] Emily M. Williamson,[1] Susan E. Habas,[2] and Richard L. Brutchey[1,*]

[1] Department of Chemistry, University of Southern California, Los Angeles, CA 90089, USA

[2] National Bioenergy Center, National Renewable Energy Laboratory, Golden, CO 80401, USA

*Email: brutchey@usc.edu

Abstract

Nanoparticles of nickel phosphide are finding wide ranging utility as catalysts for hydrodesulfurization, the hydrogen evolution reaction, and hydrodeoxygenation of bio-oils. Herein, we present a methodology to tailor monodisperse nickel phosphide nanoparticles in terms of size and phase through the use of a statistical response surface methodology (RSM). Colloidal nickel phosphide nanoparticles were synthesized by replacing octadecene (ODE), a commonly used organic solvent, by a more sustainable phosphonium-based ionic liquid (IL). The replacement of ODE with the phosphonium-based IL resulted in faster crystallization at lower temperatures to yield phase-pure, monodisperse Ni_2P nanoparticles. Using a first-order design, the PPh_3:Ni precursor ratio was identified as the most critical factor influencing the resulting size and phase of the nanoparticles. Optimization using a Doehlert matrix for second-order design yielded a second-degree polynomial equation used to predict the mean diameter of the nanoparticles (over a range of 4-12 nm) as a function of the PPh_3:Ni precursor ratio and the temperature used during synthesis. The resulting model was validated by performing reactions using randomly chosen sets of conditions; the experimentally determined nanoparticle sizes were in excellent agreement with the theoretical sizes predicted by our model. This demonstrates the utility of multivariate experimental design as a powerful tool in the development of synthetic strategies towards the preparation of colloidal nanoparticles with highly controlled size, size distribution, and phase.

Introduction

Transition metal phosphide nanoparticles have been under intensive study for more than 15 years because of their advanced catalytic properties,[1,2] particularly with respect to hydrodesulfurization (HDS),[3–9] the hydrogen evolution reaction (HER),[10] and the hydrodeoxygenation (HDO) of bio-oils.[11] One of the most studied materials within this group are the nickel phosphides, with Ni_2P generally being the most attractive phase for catalysis; however, because of the complexity of the binary Ni–P phase diagram, nanoparticles of other less desirable compositions, such as $Ni_{12}P_5$, Ni_5P_4, and NiP_2 are often observed.[12–14] Colloidal Ni_2P nanoparticles are generally prepared via the high-temperature reaction between Ni^0 or Ni^{2+} precursors and trioctylphosphine (TOP) in high-boiling organic solvents (e.g., 1-octadecene (ODE) or dioctyl ether).[12,13,15–19] As compared to TOP, triphenylphosphine (PPh_3) is less expensive (~15% of the cost of TOP in price per mole) and generally leads to nanoparticles that are larger, amorphous, and/or phase impure.[14,20] However, it was recently demonstrated by some of us that a $Ni(PPh_3)_2(CO)_2$ precursor can be reacted with excess PPh_3 in oleylamine and ODE to yield high-quality 11-nm solid nanoparticles of phase-pure Ni_2P.[21]

Over the last few years, ionic liquids (ILs) have become interesting alternatives to traditional organic solvents for the colloidal synthesis of nanoparticles since they have the potential of inducing

high nucleation rates, resulting in more monodisperse nanoparticle ensembles.[22] It has further been demonstrated that ILs can stabilize nanoparticle surfaces through a combination of their ionic nature, high dielectric constants, and ability to form liquid-phase supramolecular networks.[23–25] Moreover, ILs have excellent solvent properties such as the ability to dissolve a wide variety of solutes, and they possess a negligible vapor pressure and high thermal stability.[25] Consequently, they are promising solvents for large-scale nanofabrication reactions since they represent a safer and more environmentally friendly option over volatile and flammable organic solvents.[23] Recently, Zhang et al. reported the microwave-driven synthesis of nickel phosphide nanoparticles in a phosphonium-based IL simultaneously used as solvent and phosphide source,[26] although no specific control over size was achieved and, therefore, the corresponding nanoparticles were quite large and polydispersed. In another recent study, our group reported the synthesis of Ni_2P nanoparticles in an imidazolium-based IL that served as a phase-directing agent to produce 5-nm solid nanoparticles that were subsequently employed as catalysts for HER.[27] To the best of our knowledge, these are the only two studies on the synthesis of nickel phosphide nanoparticles in ILs thus far. Hence, the development of a general synthetic approach that allows for a careful and accurate tuning of the composition, size, and size distribution of nickel phosphide nanoparticles in IL solvents remains an outstanding challenge in the fabrication of these materials. Possessing a high degree of synthetic control will allow for morphology-function properties of these colloidal nanoparticles to be assessed; for example, the catalytic activity of Ni_2P nanoparticles have been suggested to exhibit a particle or grain size effect for several reactions.[7,28,29]

Colloidal nanoparticle syntheses, as with much of synthetic materials chemistry, has traditionally been driven by empirical discoveries achieved through one variable at a time (OVAT) optimizations. However, the complexity, variety, and correlated characteristics of experimental variables relevant to nanoparticle syntheses (including time, temperature, reaction volume, concentration, precursor ratios, order of addition, etc.) renders the OVAT approach extremely limited,[30] not only by speed, but also in optimizing the characteristics of the nanoparticle system in question. The OVAT methodology lacks the ability to elucidate and quantify the magnitude of interactions between experimental variables that affect a specific response of the nanoparticles;[31–33] therefore, multivariate experimental design techniques have the potential to make a large impact in this area of research. The use of statistical design of experiment (DoE) allows the simultaneous variation of the magnitude of a certain number of factors suspected to be determinant for a specific response, such as nanoparticle size, to determine how those factors behave separately and together while minimizing the influence of experimental error. The first stage of statistical DoE involves the detection of influential experimental variables through first-order designs (e.g., factorial designs, fractional factorial designs, or Plackett-Burman designs).[34] Once these variables have been screened, optimization through second-order designs can occur.[35,36] Response surface methodology (RSM) is among the most relevant second-order multivariate techniques used during optimization of a process and corresponds to a collection of mathematical and statistical techniques based on the fit of a polynomial equation to the experimental data with the objective of making statistical predictions.[36] The resulting equation, also known as the response surface function (RSF), enables the determination of an absolute optimum in a studied domain. The study of Burrows et al. is, to our knowledge, the only one so far using this kind of methodology to achieve control in metal nanoparticle synthesis. In that study, DoE was employed to screen seven potential factors and their associated interactions that govern the seed-mediated silver-assisted synthesis of gold nanorods.[37]

Herein, we utilize a statistics-based DoE methodology to tailor the synthesis of nickel phosphide nanoparticles in terms of size, size distribution, and phase using an RSF optimization. Nickel phosphide nanoparticles are synthesized according to the previous report of Habas et al.,[21] but replacing ODE with a phosphonium-based IL, constituted by the trihexyl(tetradecyl)phosphonium ($P[6,6,6,14]^+$) cation and bis-2,4,4-(trimethylpentyl) phosphinate as the counteranion, to determine the effect of the IL when compared to the more traditional solvent ODE on the size, the size distribution and the phase of the resulting nickel phosphide nanoparticles.

Experimental Section

Materials and methods

All chemicals and reagents were used as received without any further purification. Trihexyl(tetradecyl)phosphonium bis-2,4,4-(trimethylpentyl)phosphinate (≥95%, CYPHOS® 104), triphenylphosphine (≥99%, PPh_3), trioctylphosphine (97%, TOP) and oleylamine (70%, OAm) were purchased from Sigma-Aldrich. Trihexyl(tetradecyl)phosphonium bis(trifluoromethylsulfonyl)amide (≥98%, CYPHOS® 109) was purchased from IoLiTec. Triphenylphosphine was stored in a N_2-filled glovebox. CYPHOS® 104, CYPHOS® 109, TOP, and OAm were dried prior to use by heating them to 100 °C under vacuum for 12 h. The bis(triphenylphosphine)dicarbonylnickel complex ($Ni(PPh_3)_2(CO)_2$) and the nickel(II) acetylacetonate ($Ni(acac)_2$) were purchased from Alfa Aesar and stored in a N_2-filled glovebox. All nanoparticle syntheses were performed under a N_2 atmosphere using standard Schlenk techniques.

Synthesis of nickel phosphide nanoparticles in CYPHOS® 104

In a three-neck round bottom flask fitted with a condenser, a stopper and a septum, $Ni(PPh_3)_2(CO)_2$ (0.32 g, 0.50 mmol) and PPh_3 (0.132-2.239 g, 0.500-8.50 mmol) were mixed with dried OAm (1.7 or 3.4 mL, 7.5 or 15 mmol) and dried IL (3.0 or 6.0 mL) and the solution was heated rapidly to the desired reaction temperature (270, 305, 320 or 340 °C) at ca. 10 °C/min, and maintained there for a corresponding reaction time (3, 6, 10, 30, 60, 90 or 120 min).

In all cases, the resulting reaction mixture was removed from the heat source and naturally cooled down to room temperature upon completion. Then, 4-7 mL of hexanes and 2-5 mL of $CHCl_3$ were added to the reaction mixture in air followed by sonication for 5 min. Approximately 6-10 mL of 2-propanol were added to the solution to flocculate the particles, which were then separated by centrifugation at 4025 xg for 5 min. The isolated nanoparticles were washed a second time by replacing the colorless supernatant with fresh $CHCl_3$ (3.5 mL) and fresh hexanes (1.5 mL). This dispersion was then sonicated again (5 min) followed by the addition of 2-propanol (10 mL) and centrifugation (4025 xg for 5 min) to precipitate the nanoparticles. The isolated yield of the resulting Ni_2P nanoparticles ranged between 59-71% relative to the $Ni(PPh_3)_2(CO)_2$ precursor for 5.2 and 9.6 nm particles, respectively, as assessed by organic content-corrected thermogravimetric analysis. The nanoparticles were redispersed in 8 mL of $CHCl_3$ and sonicated once more for 5 min. A 4 mL portion of the resulting dispersion was isolated for TEM analysis. The remaining solution was then dried under flowing N_2, redispersed in 1 mL of $CHCl_3$ and drop-cast on a zero-diffraction plate for powder X-ray diffraction (XRD) analysis.

Experimental screening design and surface response methodology

The influence of a different number of experimental variables that could have a significant effect on the size, size distribution, and phase of the obtained nickel phosphide nanoparticles was determined based on a two-level fractional factorial design (i.e., first-order design). The evaluated factors and their real and coded values are reported in Table S1 and correspond to the PPh_3:Ni precursor ratio, the OAm:Ni ratio, the temperature, the time, the ramping rate, and the volume of IL employed during synthesis. Once the non-determining (inert) factors were screened out, a surface response optimization was performed through a Doehlert design (i.e., second-order design) using only size and monodispersity as the targeted responses since the phase corresponds to a categorical variable that cannot be quantified through an RSF. The construction, analysis of variance (ANOVA), and multiple linear regressions of both the first- and second-order designs were performed with the Statgraphics Centurion XVI software (Statistical Graphics, Rockville, MD, USA). All the Pareto charts, the normal probability plots, and the surface response function plots were also obtained through the former. A more detailed description of the use of first- and second-order design is given throughout the Supporting Information.

Characterization

Powder X-ray diffraction (XRD) patterns were collected in the 30-90° 2θ range using a Rigaku Ultima IV diffractometer functioning at 44 mA and 40 kV. Cu $K\alpha$ radiation (λ=1.5406 Å) and a silicon zero-diffraction substrate were employed. Transmission electron microscopy (TEM) was performed on a JEOL JEM-2100 electron microscope at an operating voltage of 200 kV, equipped with a Gatan Orius CCD camera. Samples for TEM analysis were prepared by drop casting $CHCl_3$ dispersions of the nanoparticles onto copper grids (Carbon type-B, 200 mesh, Ted Pella). TEM micrographs were processed in *Image J* (http://rsbweb.nih.gov/ij) to analyze nanoparticle size statistics. Average diameters and standard deviations were derived by measuring a minimum of N = 300 individual particles per sample averaged over multiple images and were calculated based on the major diameter of the ellipse.

Results and Discussion

Preliminary Reactions

Previously, Habas et al. reported the reaction between $Ni(PPh_3)_2(CO)_2$ and PPh_3 in OAm and ODE at 320 °C for 2 h to yield solid, crystalline Ni_2P nanoparticles using a PPh_3:Ni precursor ratio of 6.[21] Under these conditions, the nucleation of amorphous Ni-P nanoparticles takes place around 250 °C and these particles then crystallize at 320 °C into the hexagonal Ni_2P phase with a minor fraction of $Ni_{12}P_5$, as indicated by a shoulder at 49.0° 2θ corresponding to the 100% intensity (312) reflection of $Ni_{12}P_5$ (PDF#00-022-1190). After aging for 2 h at 320 °C, the minor $Ni_{12}P_5$ phase was converted into phase-pure Ni_2P. With lower PPh_3:Ni precursor ratios, a mixture of $Ni_{12}P_5$/Ni_2P was instead obtained.

The replacement of ODE by the IL solvent CYPHOS® 104, while maintaining a PPh_3:Ni precursor ratio of 6, resulted in the much faster formation of phase-pure Ni_2P phase nanoparticles at lower temperatures, as can be seen from Figure 1. A color transition from pale yellow to black is observed through the temperature range of 150 to 250 °C, which is indicative of nanoparticle nucleation and growth. In CYPHOS® 104, the nucleation of a Ni-P amorphous intermediate also arises around 250 °C, but crystallization is induced at temperatures as low as 270 °C in only 6 min. At this point, the nanoparticles display clear diffraction peaks by XRD at 40.8°, 44.6°, 47.3°, 54.2°, and 54.9° 2θ, which correspond to the (111), (201), (210), (300), and (211) reflections of phase-pure Ni_2P (PDF# 00-003-0953), respectively. Moreover, no minor fraction of $Ni_{12}P_5$ was detected during these experiments, indicating that if the formation of this crystalline phase occurs, it is only present as a transient intermediate in the first stages of the reaction. This is in agreement with our previous observation on the evolution of the Ni_2P phase in the imidazolium-based IL solvent (1-butyl-3-methylimidazolium bis(trifluoromethylsulfonyl)imide) through an amorphous-to-crystalline transition that leads directly to the crystalline Ni_2P phase.[27] Interestingly, both bis-2,4,4-(trimethylpentyl) phosphinic acid and CYPHOS® 104 have been reported as Co(II) extractants in the presence of Ni(II), and although the extraction of the former is in all cases favored over the extraction of nickel, a low extraction yield is also observed for this particular cation.[38,39] Consequently, a certain degree of interaction between the bis-2,4,4-(trimethylpentyl) phosphinate anion and the nickel phosphide is to be expected as nucleation and growth occur. Therefore, this result supports the previous implication that the IL serves as a phase directing agent through its interaction with the nanoparticle surface,[27] influencing both nucleation, growth, and crystallization.

TEM analysis of this set of reactions reveals the formation of solid and spherical nanoparticles even at 250 °C, with an increase in size while phosphidation and crystallization take place to finally produce 10.9 ± 0.52 nm Ni_2P nanoparticles (Figure S1). A control reaction performed under the same conditions with respect to time and temperature in ODE shows the formation of $Ni_{12}P_5$ nanoparticles instead of Ni_2P (Figure 1). This is in agreement with previous reports indicating crystalline $Ni_{12}P_5$ as an intermediate phase for the production of pure-phase Ni_2P nanoparticles in ODE,[40] and the requirement of more forcing conditions to achieve the Ni_2P phase under those reaction conditions.

Likewise, adding no additional PPh_3, and with lower PPh_3:Ni precursor ratios (i.e., PPh_3:Ni < 6), also yielded mixed-phase $Ni_{12}P_5/Ni_2P$ nanoparticles in CYPHOS® 104, as can be seen in Figure S2 for the kinetic study of a PPh_3:Ni = 3 synthesis. We take this as evidence that CYPHOS® 104 is not behaving as a significant phosphide source, as has been posited previously in microwave reactions.[26]

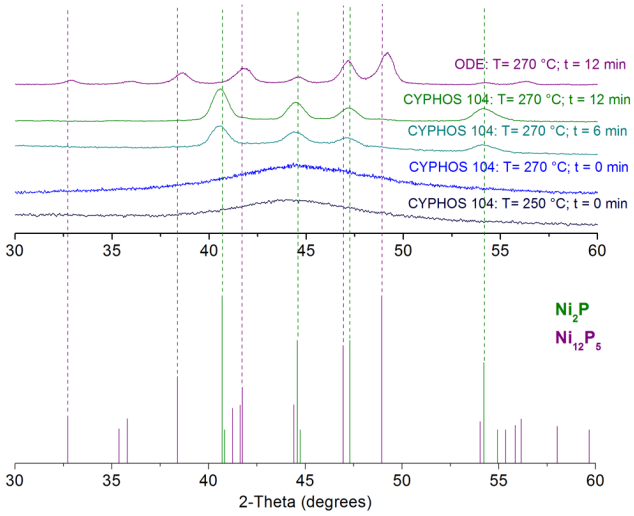

Figure 1. XRD patterns of purified samples from the different experiments performed on the effect of time and temperature in the reaction between $Ni(PPh_3)_2(CO)_2$ and PPh_3 in CYPHOS® 104 or ODE in the presence of OAm. Reference patterns are shown below and dotted lines on the experimental patterns indicate the main diffraction peaks for Ni_2P and $Ni_{12}P_5$. In all cases, PPh_3:Ni = 6, OAm:Ni = 15, ramping rate = 20 °C/min, and V_{IL} = 3 mL.

Response Surface Methodology

Normally, the first step in RSM is to screen the main factors that may affect the process of interest (in this case, the size-controlled synthesis of phase-pure Ni_2P nanoparticles) through a first-order (screening) design. Once the factors that are suspected to be relevant for the targeted responses have been identified, it is necessary to determine the sensible limits for each of these factors; that is, establishing the overall scale of the experimental design. To this end, the aforementioned preliminary reactions were performed to produce the list of conditions that define the experimental domain under study in the first-order design, which in turn allows the scaling of the second-order optimization design (vide infra). The scale of the experimental design and, therefore, the set of experiments used to build the first-order design were based on both the results of the preliminary reactions and the list of factors (Table S1) that were suspected to have a main effect on both the size and the phase of the nickel phosphide nanoparticles. When combinations of k factors are investigated at N number of levels, a full factorial design will consist of the N^k combinations that are possible and that constitutes the full set of experiments. Since, in this first stage of DoE, the main objective is to be able to discard the inert factors and, therefore, minimize the number of experiments needed for the final optimization, the set of experiments are performed using only two levels per factor. Using this minimum number of levels can only yield a first-order equation through a multiple linear regression that depicts the linear influence of the variables on the targeted response. Consequently, the resulting designs are called first-order designs. This linear equation allows the relevance of the listed factors to be assessed, as well as their statistical significance, through ANOVA. The design matrix of two fractions of a full factorial first-order design is reported in Table S2 along with the standardized Pareto charts (Figures S3 and S4) and normal probability plots (Figures S5 and S6) obtained after analysis. The standardized Pareto chart can be used to quickly determine which factors are statistically relevant. The length of each bar is proportional to the value of a t-statistic

calculated for the corresponding effect and any bars beyond the vertical error line represent statistically significant factors at a determined significance level (5% in our case). Likewise, the normal probability plot represents a complementary tool to assess which are the statically relevant factors for a specific response. When the data from a specific design occurs simply as the result of random variation about a mean and the changes in levels of the *k* factors have no real influence on the response, the effects representing the corresponding contrasts between the different pairs of responses will have roughly normal distributions centered at zero and will plot on a normal probability plot scale as a straight line called the "error line". However, when the effects fall off such line, they are not easily explained as chance occurrences and are mainly a consequence of a significant statistical influence on the corresponding response. In our case, the results of the corresponding analysis clearly point to the PPh_3:Ni precursor ratio as the main factor for controlling both the phase and the size of the nanoparticles, and demonstrate that an increase in the PPh_3:Ni ratio favors the formation of small, pure-phase Ni_2P nanoparticles. Indeed, PPh_3 not only behaves as a phosphide source but has also been proven to act as a strong surface ligand in the same manner as TOP in the synthesis of Ni nanoparticles.[41] Consequently, it could be assumed that an increase in the PPh_3 concentration can arrest growth through an increased stabilization of the nanoparticle surface.[18,42] Likewise, time and temperature seem to have a slight effect on the nanoparticle size and crystal phase; longer times promote the formation of the hexagonal Ni_2P phase while higher temperatures produce smaller nanoparticles. Nonetheless, the value of the PPh_3:Ni precursor ratio standardized effect is almost two times the standardized effects of temperature and time, and it is the only factor that shows a contribution with a p-value < 0.05.

As previously mentioned, the use of first-order designs during the screening of influential factors normally requires only two levels for each factor to achieve a fast determination of the critical variables by employing the minimum number of experiments. However, since only two levels are used, the models that can be fit to these designs are somewhat restricted (i.e., only linear equations can be obtained that normally cannot fully describe the dependency of the response on the critical variables). Consequently, to perform an optimization of the experimental conditions after spotting the statistically relevant factors, one must resort to second-order designs (i.e., response surface methodologies), which employ numerous levels per factor to allow the best fitting of a full polynomial function. A practical, effective, and versatile second-order design is the uniform shell design proposed by Doehlert in 1970 that normally requires fewer experiments than more traditional designs (Box-Behnken and Central Composite designs), and can be equally or even more effective.[43,44] One of the most interesting characteristics of Doehlert matrices when compared to the more traditional second-order designs (i.e. the three level factorial designs, the central composite designs, and the Box-Behnken designs) is that they involve different numbers of levels for each of the critical factors. As a result, some influential variables can be studied in more detail than the rest without increasing the numbers of experiments. In this study, the best system performance was achieved through an RSM based on a Doehlert matrix (Table 1). Based on the results of the ANOVA of the first-order design, the PPh_3:Ni precursor ratio was considered as a main factor and temperature as a secondary factor, using five and three different levels per factor, respectively, to achieve size optimization for the nanoparticles. The reaction time was fixed to 60 min for this set of experiments since the previous first-order design shows a slight positive effect on the Ni_2P phase with increasing time. However, phase-pure Ni_2P nanoparticles can be attained in only a few minutes (Figure 1), and the effect of this factor is not expected to be as significant as the effect of the PPh_3:Ni precursor ratio. The employed Doehlert matrix (Table 1) illustrates the variation of the PPh_3:Ni precursor ratio within the range of 3-19 with a 4 unit increment between each level (Table S3), and the variation of the temperature within the range 270-340 °C with a 35 °C unit increment between each level (Table S4). Replicates at the central level of the variables (Exps. 4b and 4c in Table 1) were performed in order to validate the model by means of an estimate of the experimental variance. A more detailed description of the use of first- and second-order design is given throughout the Supporting Information.

Once the set of experiments were performed, and both the size and the coefficient of variance (CV) were determined through the corresponding TEM images, the resulting Pareto chart (Figure S7)

showed a strong influence of the PPh_3:Ni precursor ratio on the size of the nickel phosphide nanoparticles since the bar related to the standardized effect of such factor, as well as the one related to its quadratic interaction (AA), are above the vertical line. Equation 1 describes the dependence of the size of Ni_2P nanoparticles as a function of the real values of the variables of temperature and PPh_3:Ni precursor ratio:

$$Size = 24.15 - 1.5\ PPh_3{:}Ni + 0.045\ PPh_3{:}Ni^2 + 8.2 \times 10^{-5}\ Temp^2 + 3.6 \times 10^{-4}\ PPh_3{:}Ni * Temp - 0.055\ Temp \quad (\mathbf{1})$$

The same equation in terms of the coded values of the variables is also reported in the Supporting Information (Equation S2). In DoE, codifying the variables serves a very specific purpose – since all the variables are normalized, the relative change of a variable is directly related to the size of its regression coefficient. Therefore, only the equation using the coded values can be used to compare the absolute effect of the variables on the size of the nanoparticles. This means that if the model parameters have a large absolute value, the corresponding variable has a significant effect on the response. Consequently, the difference between the order of magnitude of the coefficients in the coded equation, when compared to the real values equation, is just a consequence of the differences in terms of the magnitude of scales between the two variables (PPh_3:Ni *vs* temperature). Notably, the resulting size of the nanoparticles displays a quadratic dependence on the PPh_3:Ni precursor ratio, and the coefficient of the quadratic term in the coded equation (Equation S2) is only slightly less than that of the associated linear PPh_3:Ni precursor ratio term. Consequently, the quadratic term induces the curvature observed in the RSF plotted in Figure 2. The contours of the estimated RSF (Figure 2) were obtained from Equation S2. The ANOVA and the normal probability plot (Figure S8) of the effects validate the above conclusions since the effect of the PPh_3:Ni precursor ratio and its quadratic interaction fall off the error line. A correlation coefficient adjusted by degrees of freedom of 94.4% and analysis of residuals, which show a random pattern (Figure S9), confirm the validity of our model. Figure 3 shows the evident effect of the increase on the PPh_3:Ni precursor ratio on the size of phase-pure Ni_2P nanoparticles observed through the TEM images. It is worth noting the products obtained from experiment 1a are the only nanoparticles that were not phase pure, as this PPh_3:Ni precursor ratio leads to mixed-phase $Ni_2P/Ni_{12}P_5$ nanoparticles. However, phase-pure Ni_2P nanoparticles were produced in all the remaining cases.

Table 1. Doehlert matrix employed for studying the simultaneous effects of the PPh_3P:Ni precursor ratio and the reaction temperature on the mean size and monodispersity of the nickel phosphide nanoparticles. Real and coded values (in parenthesis) of the variables are indicated. Also displayed are the experimentally measured diameters of the nanoparticles resulting from each set of conditions and the corresponding coefficient of variance (CV).

Experiment	PPh_3:Ni	T (°C)	Size (nm)	CV (%)
1a	3 (-1)	305 (0)	11.6	9.8
2a	7 (-0.5)	270 (-0.866)	7.4	6.1
3a	7 (-0.5)	340 (0.866)	7.2	6.1
4a	11 (0)	305 (0)	5.4	6.1
4b	11 (0)	305 (0)	5.3	8.2
4c	11 (0)	305 (0)	5.3	6.8
5a	15 (0.5)	340 (0.866)	5.0	8.3
6a	15 (0.5)	270 (-0.866)	5.0	6.7
7a	19 (1)	305 (0)	4.8	5.1

The same analysis was applied using the CV as the variable response to study the effect of both the PPh_3P:Ni precursor ratio and the temperature on the polydispersity of the nanoparticles; although, in all cases the resulting nanoparticles are monodisperse, and therefore no significant effect of the PPh_3P:Ni precursor ratio nor the temperature was observed for this specific response (Figure S10).

The surface generated by second-order designs such as the Doehlert design can be used to calculate the coordinates of critical points of the RSF characterized by a maximum, a minimum, or a saddle.[36] In this case, it was found that the smallest size for phase-pure Ni_2P nanoparticles should be achieved with a PPh_3:Ni precursor ratio of 15.2 and a reaction temperature of 304.5 °C. Therefore, aiming to experimentally validate our model, the reaction between $Ni(PPh_3)_2(CO)_2$ and PPh_3 in CYPHOS® 104 and OAm was performed under this PPh_3:Ni precursor ratio and temperature. In addition, another arbitrary point of the RSF described by Equation 2 was chosen to further validate our model. The corresponding experimental results and their replicates are shown in Table 2 and Figure 4 and are in excellent agreement with the theoretical size values predicted by our model.

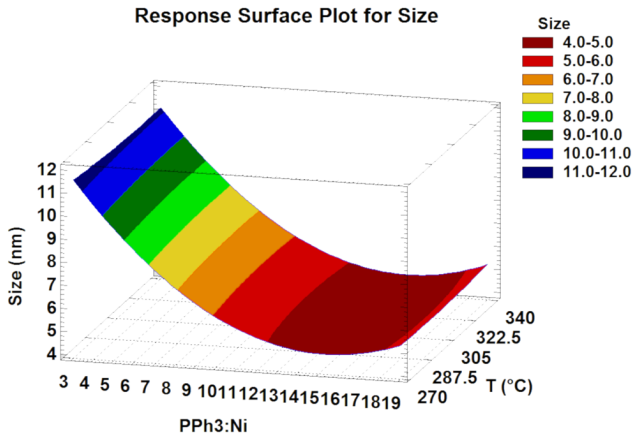

Figure 2. Calculated response surface function plotted to illustrate the dependence of the size of monodisperse nickel phosphide nanoparticles as a function of the PPh_3:Ni precursor ratio and temperature.

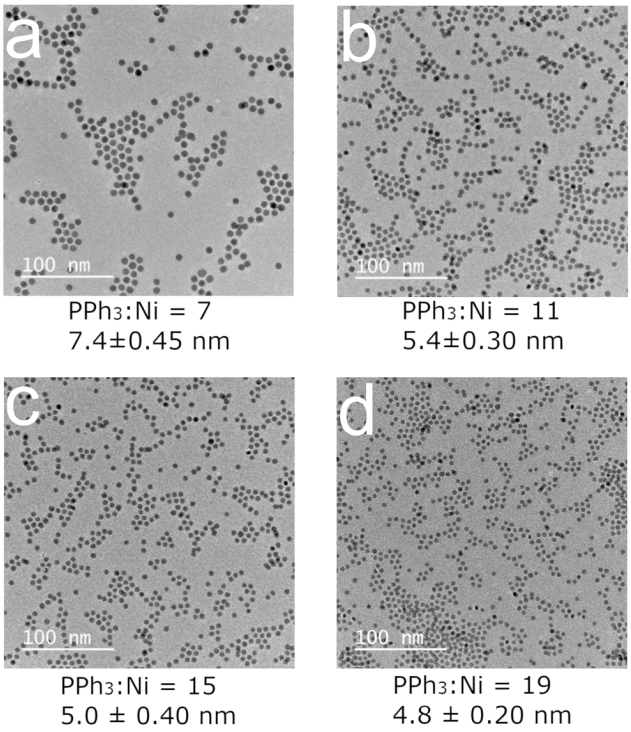

Figure 3. Effect of the PPh_3:Ni precursor ratio on the size of phase-pure Ni_2P nanoparticles obtained in experiments (a) 2a, (b) 4a, (c) 5a, and (d) 7a. In all cases OAm:Ni = 15, t = 60 min, ramping rate = 20 °C/min, and V_{IL} = 3 mL.

Table 2. Experiments for corroborating the model described in Eq. 2

Experiment	PPh_3:Ni	T (°C)	Predicted Size (nm)	Real Size (nm)
8a	15.2	304.5	4.5	4.8 ± 0.3
8b	15.2	304.5	4.5	4.8 ± 0.2
9a	8.0	290.0	6.9	6.9 ± 0.4
9b	8.0	290.0	6.9	6.6 ± 0.4

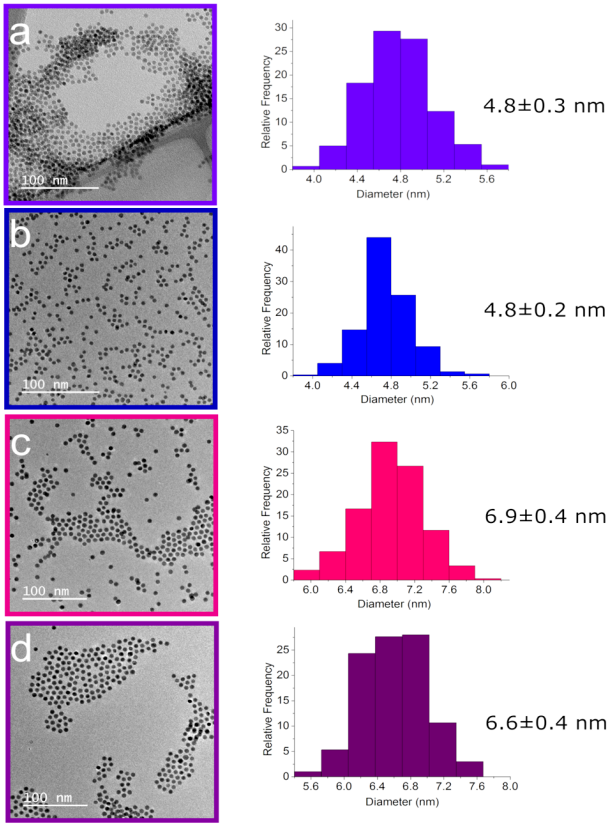

Figure 4. TEM images and corresponding size distributions for the conditions reported in Table 2 for the validation of the model. Experiments (a) 8a, (b) 8b, (c) 9a, and (d) 9b. In all cases, OAm:Ni = 15, t = 60 min, ramping rate = 20 °C/min, and V_{IL} = 3 mL.

Subsequent Reactions

A number of subsequent reactions were performed under PPh_3:Ni precursor ratios and reaction temperatures that lead to phase-pure Ni_2P nanoparticles in CYPHOS® 104. The main goal of such reactions was to gain some additional insight into the role of the IL during the nickel phosphide nanoparticle synthesis. It is worth noticing that a striking result, besides the fast kinetics of the reaction, is the consistent monodispersity of the nanoparticles throughout all the experiments shown in the previous sections. Particularly because such effects are characteristic of the use of the IL as solvent during the reaction and are not observed in the most traditional solvent ODE.[21]

Aiming to assess the role of the bis-2,4,4-(trimethylpentyl) phosphinate anion in the nucleation and growth of the nickel phosphide nanoparticles, a control reaction was performed using an analogous phosphonium-based IL, CYPHOS® 109, constituted by the same cation but containing the the weakly coordinating bis(trifluoromethylsulfonyl)amide anion instead. The XRD pattern given in Figure 5a shows the formation of phase-impure nickel phosphide nanoparticles rather than phase-pure Ni_2P nanoparticles when CYPHOS® 104 is replaced by CYPHOS® 109 under otherwise identical conditions. Likewise, TEM analysis reveals the formation of solid but polydisperse nanoparticles after a 60 min reaction time when CYPHOS® 104 is replaced by CYPHOS® 109 (Figure S11).

Therefore, the presence of the bis-2,4,4-(trimethylpentyl) phosphinate anion appears to have a strong influence on the size, phase, and size distribution of the resulting nanoparticles. This could be a consequence of the more weakly coordinating effect of the bis(trifluoromethylsulfonyl)amide anion on the nickel intermediate. Moreover, it reveals the role of the bis-2,4,4-(trimethylpentyl) phosphinate anion on the stabilization of the nanoparticles as nucleation and growth takes place. In

a second experiment, PPh_3 was replaced by TOP to establish the role of the phosphide source in the kinetics of the reaction. The XRD pattern in Figure 5a for this reaction shows the formation of a Ni-P amorphous intermediate instead of phase-pure Ni_2P nanoparticles. Consequently, PPh_3 can be thought as more reactive phosphide source in CYPHOS® 104 when compared with TOP, which will lead to the much faster formation of phase-pure Ni_2P nanoparticles.

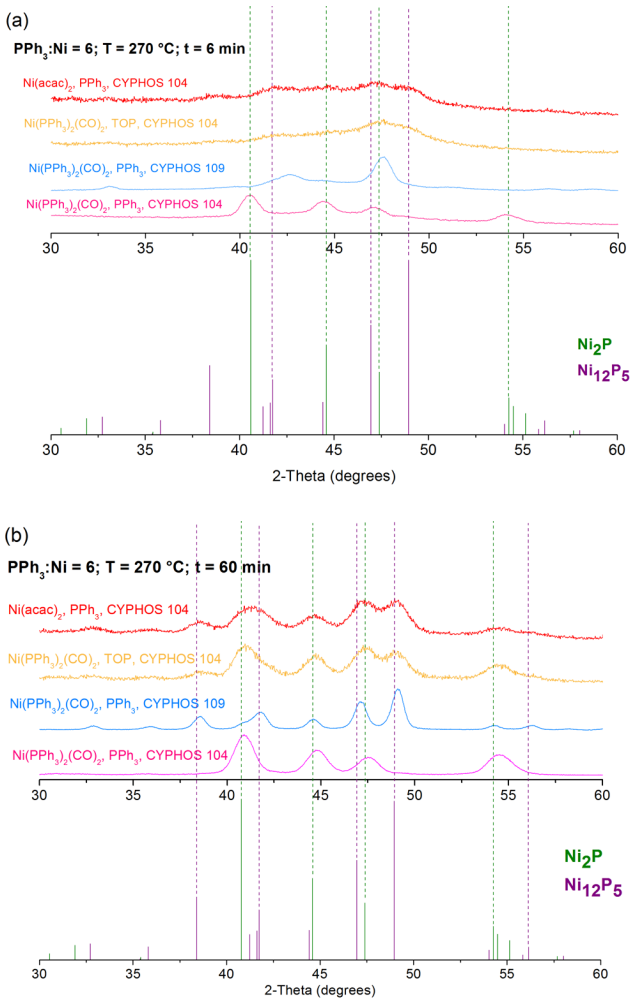

Figure 5. XRD patterns of purified samples of the different experiments performed on the effect of the nature of the IL anion, the phosphide source, and the nature of the nickel precursor in the synthesis of nickel phosphide nanoparticles (a) after 6 min of reaction and (b) after 60 min of reaction. Reference patterns are shown below and dotted lines on the experimental patterns indicate the main diffraction peaks for Ni_2P and $Ni_{12}P_5$. In all cases, PPh_3:Ni = 6, T = 270 °C, OAm:Ni = 15, ramping rate = 20 °C/min, and V_{IL} = 3 mL.

Finally, the effect of the nature of the metal precursor was investigated by replacing $Ni(PPh_3)_2(CO)_2$ with $Ni(acac)_2$. In this case, crystallization of the Ni_2P nanoparticles cannot be achieved within 6 min at 270 °C. Hence, the structural characteristics and reactivity of the $Ni(PPh_3)_2(CO)_2$ precursor, where PPh_3 is pre-coordinated to the Ni center, promote faster crystallization during the formation of the nanoparticles. The same set of experiments was performed using a 60 min reaction time under otherwise identical conditions (Figure 5b). From Figure 5b it can be seen that the formation of phase-pure Ni_2P nanoparticles is a consequence of a synergistic effect

between the stabilizing ability of the phosphinate anion, the use of PPh_3 as a more reactive phosphide source, and the fact that the latter is also contained within the structure of the $Ni(PPh_3)_2(CO)_2$ precursor.

Electrocatalysis

In order to assess the catalytic viability of Ni_2P nanoparticles synthesized in CYPHOS® 104, the particles were tested for HER and compared to particles prepared by the standard preparation in ODE. The working electrodes were prepared by drop-casting colloidal suspensions of Ni_2P nanoparticles onto carbon paper to achieve a mass loading of 1 mg/cm^2, followed by heating to 450 ˚C under forming gas (5% H_2/95% N_2) to clean and reduce the catalyst surface. A typical three-electrode cell was used with 0.5 M H_2SO_4. Polarization data were obtained for 5.2 and 9.6 nm Ni_2P particles synthesized in CYPHOS® 104, Ni_2P nanoparticles prepared in ODE according to a literature procedure,[21] and bare carbon paper as the working electrode (Figure S12). The small and large Ni_2P particles synthesized in CYPHOS® 104 were found to be catalytically active for HER and exhibited comparable overpotentials of $\eta_{-10\ mA/cm^2}$ = -178 and -175 mV, respectively. The bare carbon paper did not exhibit any substantial activity for HER over the potential range measured. In comparison, the Ni_2P nanoparticles synthesized in ODE exhibited an overpotential of $\eta_{-10\ mA/cm^2}$ = -148 mV. The Tafel slopes were 64 and 61 mV/dec for the small and large Ni_2P particles synthesized in CYPHOS® 104, respectively, as compared to 59 mV/dec for the particles prepared in ODE (Figure S13). The measured values are comparable to Ni_2P nanoparticle-modified electrodes reported in the literature with similar mass loadings.[45,46] Importantly, these results clearly demonstrate that synthesizing the Ni_2P nanoparticles in CYPHOS® 104 does not render them catalytically inactive for HER, as we have previously demonstrated for Ni_2P nanoparticles synthesized in imidazolium-based ILs.[27]

Conclusions

Nickel phosphide nanoparticles have been synthesized by replacing ODE with a phosphonium-based IL constituted by the trihexyl(tetradecyl)phosphonium ($P[6,6,6,14]^+$) cation and bis-2,4,4-(trimethylpentyl) phosphinate as the counteranion. Oleylamine and PPh_3 were used as the stabilizing ligand and phosphide source, respectively. The replacement of the more traditional ODE solvent with the phosphonium-based IL induced crystallization at 270 °C in only 6 min and resulted in the much faster formation of phase-pure, solid, monodisperse Ni_2P nanoparticles. Moreover, no minor fraction of the $Ni_{12}P_5$ phase was detected during early stages of the reaction, indicating that evolution of the Ni_2P phase in CYPHOS® 104 occurs through an amorphous-to crystalline transition that leads directly to the crystalline Ni_2P phase. Likewise, based on the nature of the IL, a certain degree of interaction between the bis-2,4,4-(trimethylpentyl) phosphinate anion and the nickel phosphide nanoparticles is to be expected as nucleation and growth occur. The use of a first-order design determined the PPh_3:Ni ratio to be the most critical factor in the resulting size and phase of the nanoparticles. Optimization using a Doehlert matrix for second-order design produced a second-order polynomial equation used to predict the size of the nanoparticles in terms of the PPh_3:Ni ratio and the temperature employed during synthesis. This expression enabled the predictable tuning of the size of pure-phase, solid, monodisperse Ni_2P nanoparticles in the 4-12 nm range. The ANOVA and the normal probability plot of the effects validate the above conclusions while a correlation coefficient adjusted by degrees of freedom of 94.4% and the analysis of residuals confirm the validity of our model. The model was further corroborated by performing the reaction under optimum conditions, and by using a random set of conditions. The results obtained are in excellent agreement with the theoretical size values predicted by our model, highlighting the scope of multivariate experimental design techniques in the optimization of colloidal nanoparticle syntheses. Finally, the fast kinetics and the formation of monodisperse nickel phosphide nanoparticles was proven to be a synergetic effect between the coordination and stabilization ability of the bis-2,4,4-(trimethylpentyl) phosphinate anion, a high reactivity of the PPh_3 as phosphide source, and its presence within the structure of the $Ni(PPh_3)_2(CO)_2$ precursor.

■ ASSOCIATED CONTENT

Supporting Information

The Supporting Information is available free of charge on the ACS Publications website at DOI:

XRD patterns; supplemental DoE and RSM information; TEM images; HER experimental; polarization data; Tafel plots (PDF)

■ AUTHOR INFORMATION

Corresponding Author

*E-mail: brutchey@usc.edu

ORCID

Richard L. Brutchey: 0000-0002-7781-5596
Lucia Mora-Tamez: 0000-0001-5532-6866
Susan E. Habas: 0000-0002-3893-8454
Gözde Barim: 0000-0001-8139-925X
Courtney A. Downes: 0000-0001-8631-1579

Notes

The authors declare no competing financial interest.

■ ACKNOWLEDGMENTS

L.M.T. thanks the CONACyT (Mexico) for a postdoctoral fellowship (CVU 256605; REG. 216085; SOL. 477407). R.L.B. acknowledges the National Science Foundation for supporting the synthetic chemistry in ionic liquids under CMMI-1728649. This work was authored in part by S.E.H. at the National Renewable Energy Laboratory, operated by Alliance for Sustainable Energy, LLC, for the U.S. Department of Energy (DOE) under Contract No. DE-AC36-08GO28308. Funding for S.E.H. provided as part of the ChemCatBio Consortium, an Energy Materials Network Consortium funded by the U.S. DOE, Office of Energy Efficiency and Renewable Energy, Bioenergy Technologies Office. The views expressed in the article do not necessarily represent the views of the DOE or the U.S. Government.

References

[1] Prins, R.; Bussell, M. E. Metal Phosphides: Preparation, Characterization and Catalytic Reactivity. *Catal. Letters* **2012**, *142*, 1413–1436.

[2] Cao, S.; Wang, C. J.; Fu, W. F.; Chen, Y. Metal Phosphides as Co-Catalysts for Photocatalytic and Photoelectrocatalytic Water Splitting. *ChemSusChem* **2017**, *10*, 4227.

[3] Korányi, T. I. Phosphorus Promotion of Ni (Co)-Containing Mo-Free Catalysts in Thiophene Hydrodesulfurization. *Appl. Catal. A Gen.* **2003**, *239*, 253–267.

[4] Oyama, S. T.; Wang, X.; Requejo, F. G.; Sato, T.; Yoshimura, Y. Hydrodesulfurization of Petroleum Feedstocks with a New Type of Nonsulfide Hydrotreating Catalyst. *J. Catal.* **2002**, *209*, 1–5.

[5] Oyama, S. T. Novel Catalysts for Advanced Hydroprocessing: Transition Metal Phosphides. *J. Catal.* **2003**, *216*, 343–352.

[6] Sawhill, S. J.; Phillips, D. C.; Bussell, M. E. Thiophene Hydrodesulfurization over Supported Nickel Phosphide Catalysts. *J. Catal.* **2003**, *215*, 208–219.

[7] Oyama, S. T.; Lee, Y. K. The Active Site of Nickel Phosphide Catalysts for the Hydrodesulfurization of 4,6-DMDBT. *J. Catal.* **2008**, *258*, 393–400.

[8] Oyama, S. T.; Gott, T.; Zhao, H.; Lee, Y. K. Transition Metal Phosphide Hydroprocessing Catalysts: A Review. *Catal. Today* **2009**, *143*, 94–107.

[9] D'Aquino, A. I.; Danforth, S. J.; Clinkingbeard, T. R.; Ilic, B.; Pullan, L.; Reynolds, M. A.; Murray, B. D.; Bussell, M. E. Highly-Active Nickel Phosphide Hydrotreating Catalysts Prepared in Situ Using Nickel Hypophosphite Precursors. *J. Catal.* **2016**, *335*, 204–214.

[10] Popczun, E. J.; McKone, J. R.; Read, C. G.; Biacchi, A. J.; Wiltrout, A. M.; Lewis, N. S.; Schaak, R. E. Nanostructured Nickel Phosphide as an Electrocatalyst for the Hydrogen Evolution Reaction. *J. Am. Chem. Soc.* **2013**, *135*, 9267–9270.

[11] Griffin, M. B.; Baddour, F. G.; Habas, S. E.; Ruddy, D. A.; Schaidle, J. A. Evaluation of Silica-Supported Metal and Metal Phosphide Nanoparticle Catalysts for the Hydrodeoxygenation of Guaiacol Under Ex Situ Catalytic Fast Pyrolysis Conditions. *Top. Catal.* **2016**, *59*, 124–137.

[12] Li, D.; Senevirathne, K.; Aquilina, L.; Brock, S. L. Effect of Synthetic Levers on Nickel Phosphide Nanoparticle Formation: Ni_5P_4 and NiP_2. *Inorg. Chem.* **2015**, *54*, 7968–7975.

[13] Muthuswamy, E.; Savithra, G. H. L.; Brock, S. L. Control of Phase , Size , and Morphology in Nickel Phosphide Nanoparticles. *ACS Nano* **2011**, 2402–2411.

[14] Pan, Y.; Liu, Y.; Liu, C. An Efficient Method for the Synthesis of Nickel Phosphide Nanocrystals via Thermal Decomposition of Single-Source Precursors. *RSC Adv.* **2015**, *5*, 11952–11959.

[15] K. Senevirathne, A. W. Burns, M. E. Bussell, S. L. Brock, *Adv. Funct. Mater.* **2007**, *17*, 3933–3939.

[16] Park, J.; Koo, B.; Yoon, K. Y.; Hwang, Y.; Kang, M.; Park, J. G.; Hyeon, T. Generalized Synthesis of Metal Phosphide Nanorods via Thermal Decomposition of Continuously Delivered Metal-Phosphine Complexes Using a Syringe Pump. *J. Am. Chem. Soc.* **2005**, *127*, 8433–8440.

[17] Henkes, A. E.; Schaak, R. E. Trioctylphosphine: A General Phosphorus Source for the Low-Temperature Conversion of Metals into Metal Phosphides. *Chem. Mater.* **2007**, *19*, 4234–4242.

[18] Wang, J.; Johnston-Peck, A. C.; Tracy, J. B. Nickel Phosphide Nanoparticles with Hollow, Solid, and Amorphous Structures. *Chem. Mater.* **2009**, *21*, 4462–4467.

[19] Carenco, S.; Portehault, D.; Boissière, C.; Mézailles, N.; Sanchez, C. Nanoscaled Metal Borides and Phosphides : Recent Developments and Perspectives. *Chem. Rev.* **2013**, *113*, 7981–8065.

[20] Zheng, X.; Yuan, S.; Tian, Z.; Yin, S.; He, J.; Liu, K.; Liu, L. One-pot Synthesis of Hollow Nickel Phosphide Nanoparticles with Tunable Void Sizes Using Triphenylphoshine. *Mater. Lett.* **2009**, *63*, 2283–2285.

[21] Habas, S. E.; Baddour, F. G.; Ruddy, D. A.; Nash, C. P.; Wang, J.; Pan, M.; Hensley, J. E.; Schaidle, J. A. A Facile Molecular Precursor Route to Metal Phosphide Nanoparticles and Their Evaluation as Hydrodeoxygenation Catalysts. *Chem. Mater.* **2015**, *27*, 7580–7592.

[22] Antonietti, M.; Kuang, D.; Smarsly, B.; Zhou, Y. Ionic Liquids for the Convenient Synthesis of Functional Nanoparticles and Other Inorganic Nanostructures. *Angew. Chem. Int. Ed.* **2004**, *43*, 4988-4992.

[23] Welton, T. Room-Temperature Ionic Liquids. Solvents for Synthesis and Catalysis. *Chem. Rev.* **1999**, *99*, 2071–2084.

[24] Dupont, J.; Scholten, J. D. On the Structural and Surface Properties of Transition-Metal Nanoparticles in Ionic Liquids. *Chem. Soc. Rev.* **2010**, *39*, 1780.

[25] Wegner, S.; Janiak, C. *Metal Nanoparticles in Ionic Liquids*, Springer International Publishing, **2017**.

[26] Zhang, C.; Xin, B.; Xi, Z.; Zhang, B.; Li, Z.; Li, Z.; Zhang, H.; Hao, J. Phosphonium-Based Ionic Liquid: A New Phosphorus Source toward Microwave-Driven Synthesis of Nickel Phosphide for Efficient Hydrogen Evolution Reaction. *ACS Sustain. Chem. Eng.* **2018**, *6*, 1468–1477.

[27] Roberts, E. J.; Read, C. G.; Lewis, N. S.; Brutchey, R. L. Phase Directing Ability of an Ionic Liquid Solvent for the Synthesis of HER-Active Ni_2P Nanocrystals. *ACS Appl. Energy Mater.* **2018**, *1*, 1823–1827.

[28] Hsu, P. J.; Lin, Y. C. Hydrodeoxygenation of 4-Methylguaiacol over Silica-Supported Nickel Phosphide Catalysts: The Particle Size Effect. *J. Taiwan Inst. Chem. Eng.* **2017**, *79*, 80–87.

[29] Yang, Y.; Chen, J.; Shi, H. Deoxygenation of Methyl Laurate as a Model Compound to Hydrocarbons on Ni_2P/SiO_2, Ni_2P/MCM-41, and Ni_2P/SBA-15 Catalysts with Different Dispersions. *Energy and Fuels* **2013**, *27*, 3400–3409.

[30] Cao, B.; Adutwum, L. A.; Oliynyk, A. O.; Luber, E. J.; Olsen, B. C.; Mar, A.; Buriak, J. M. How To Optimize Materials and Devices *via* Design of Experiments and Machine Learning: Demonstration Using Organic Photovoltaics. *ACS Nano* **2018**, *12*, 7434-7444.

[31] Box, G. E. P.; Hunter, J. S.; Hunter, W. G. *Statistics for Experimenters. Design, Innovation, and Discovery*, Wiley-Interscience, 2005.

[32] Brereton, R. G. *Applied Chemometrics for Scientists*, John Wiley & Sons, 2007.

[33] Weissman, S. A.; Anderson, N. G. Design of Experiments (DoE) and Process Optimization. A Review of Recent Publications. *Org. Process Res. Dev.* **2015**, *19*, 1605–1633.

[34] Lundstedt, T.; Seifert, E.; Abramo, L.; Thelin, B.; Nystrom, A.; Pettersen, J.; Bergman, R. Experimental Design and Optimization. *Chemom. Intell. Lab. Syst.* **1998**, *42*, 3-40.

[35] Vera Candioti, L.; De Zan, M. M.; Cámara, M. S.; Goicoechea, H. C. Experimental Design and Multiple Response Optimization. Using the Desirability Function in Analytical Methods Development. *Talanta* **2014**, *124*, 123–138.

[36] Bezerra, M. A.; Santelli, R. E.; Oliveira, E. P.; Villar, L. S.; Escaleira, L. A. Response Surface Methodology (RSM) as a Tool for Optimization in Analytical Chemistry. *Talanta* **2008**, *76*, 965–977.

[37] Burrows, N. D.; Harvey, S. Idesis, F. A.; Murphy, C. J. Understanding the Seed-Mediated Growth of Gold Nanorods through a Fractional Factorial Design of Experiments. *Langmuir* **2017**, *33*, 1891–1907.

[38] Xun, F.; Golding, J. A. Solvent Extraction of Cobalt and Nickel in bis(2,4,4-Tri-Methylpentyl) Phosphinic Acid, “cyanex −272.” *Solvent Extr. Ion Exch.* **1987**, *5*, 205–226.

[39] Rybka, P.; Regel-Rosocka, M. Nickel(II) and Cobalt(II) Extraction from Chloride Solutions with Quaternary Phosphonium Salts. *Sep. Sci. Technol.* **2012**, *47*, 1296–1302.

[40] Andaraarachchi, H. P.; Thompson, M. J.; White, M. A.; Fan, H. J.; Vela, J. Phase-Programmed Nanofabrication: Effect of Organophosphite Precursor Reactivity on the Evolution of Nickel and Nickel Phosphide Nanocrystals. *Chem. Mater.* **2015**, *27*, 8021–8031.

[41] Park, J.; Kang, E.; Son, S. U.; Park, H. M.; Lee, M. K.; Kim, J.; Kim, K. W.; Noh, H. J.; Park, J. H.; Bae, C. J.; et al. Monodisperse Nanoparticles of Ni and NiO: Synthesis,

Characterization, Self-Assembled Superlattices, and Catalytic Applications in the Suzuki Coupling Reaction. *Adv. Mater.* **2005**, *17*, 429–434.

[42] Carenco, S.; Boissière, C.; Nicole, L.; Sanchez, C.; Le Floch, P.; Mézailles, N. Controlled Design of Size-Tunable Monodisperse Nickel Nanoparticles. *Chem. Mater.* **2010**, *22*, 1340–1349.

[43] Doehlert, D. H. Uniform Shell Designs. *J. R. Stat. Soc.* **1970**, *19*, 231–239.

[44] Ferreira, S. L. C.; Dos Santos, W. N. L.; Quintella, C. M.; Neto, B. B.; Bosque-Sendra, J. M. Doehlert Matrix: A Chemometric Tool for Analytical Chemistry - Review. *Talanta* **2004**, *63*, 1061–1067.

[45] Callejas, J. F.; Read, C. G.; Roske, C. W.; Lewis, N. S.; Schaak, R. E. Synthesis, Characterization, and Properties of Metal Phosphide Catalysts for the Hydrogen-Evolution Reaction. *Chem. Mater.* **2016**, *28*, 6017-6044.

[46] Mundy, M. E.; Ung, D.; Lai, N. L.; Jahrman, E. P.; Seidler, G. T.; Cossairt, B. M. Aminophosphines as Versatile Precursors for the Synthesis of Metal Phosphide Nanocrystals. *Chem. Mater.* **2018**, *30*, 5373-5379.